Stabilizing effect of mélange buttressing on the Marine Ice Cliff Instability of the West Antarctic Ice Sheet

Tanja Schlemm[1,2], Johannes Feldmann[1], Ricarda Winkelmann[1,2], and Anders Levermann[1,2,3]

[1]Potsdam Institute for Climate Impact Research, Potsdam, Germany
[2]Institute of Physics and Astronomy, University of Potsdam, Potsdam, Germany
[3]Lamont-Doherty Earth Observatory, Columbia University, New York, USA

Correspondence: anders.levermann@pik-potsdam.de

Abstract. Due to global warming and particularly high regional ocean warming, both Thwaites and Pine Island glaciers in the Amundsen region of the Antarctic Ice Sheet could lose their buttressing ice shelves over time. We analyze the possible consequences using the Parallel Ice Sheet Model (PISM), applying a simple cliff-calving parameterization and an ice-mélange-buttressing model. We find that the instantaneous loss of ice-shelf buttressing, due to enforced ice-shelf melting, initiates grounding line retreat and triggers the marine ice sheet instability (MISI). As a consequence, the grounding line progresses into the interior of the West Antarctic Ice Sheet and leads to a sea level contribution of 0.6 m within 100 a. By subjecting the exposed ice cliffs to cliff calving using our simplified parameterization, we also analyze the marine ice cliff instability (MICI). In our simulations it can double or even triple the sea level contribution depending on the only loosely ~~constraint parameter which~~ constrained parameter that determines the maximum cliff-calving rate. The speed of MICI depends on this upper bound ~~on~~ of the calving rate, which is given by the ice mélange buttressing the glacier. However, stabilization of MICI may occur for geometric reasons. Since the embayment geometry changes as MICI advances into the interior of the ice sheet, the upper bound on calving rates is reduced and the progress of MICI is slowed down. Although we cannot claim that our simulations bear relevant quantitative estimates of the effect of ice-mélange buttressing on MICI, the mechanism has the potential to stop the instability. Further research is needed to evaluate its role for the past and future evolution of the Antarctic Ice Sheet.

1 Introduction

Ice loss from the Greenland and Antarctic ice sheets is contributing increasingly to global sea level rise (**???**). Ice sheets gain mass through accumulation of snowfall. Whether they contribute to sea level changes depends on how much this mass gain is offset or overcompensated by mass losses due to surface and basal melting as well as iceberg calving. Both ice sheets in Greenland and Antarctica are currently losing ice (**?????**). Estimating the additional future mass loss of these ice sheets is critical for future sea level projections (**?????????**). Uncertainties in modeling the physics of the Antarctic Ice Sheet (AIS) lead to large uncertainties in sea level projections (**??**).

One such uncertainty is the potential collapse and the calving of large ice cliffs after the ice shelves buttressing them have disintegrated. The concept of cliff calving was motivated by an analysis of depth-averaged stresses near an ice cliff, which showed that ice cliffs exceeding an ice thickness stability limit are inherently unstable (**?**). Cliff calving could lead to uncontrolled ice retreat: Grounding line retreat caused by cliff calving may expose even higher ice cliffs further inland, which in turn are more susceptible to collapse, resulting in self-reinforcing ice retreat. This is referred to as Marine Ice Cliff Instability (MICI) (**?**) .
A study by **?** found that the AIS could contribute up to 1 m of sea level rise within a century, if cliff calving is taken into account. This is substantially more than all other projections that do not include MICI. However, this study has been criticised as over-estimating sea level contribution (**?**) due to a lack of observationally constrained models of the cliff calving process. **?** parameterized cliff calving with a step-like function that is zero for ice cliffs below the stability limit and ramps up rapidly to an upper limit for all ice cliffs exceeding the stability limit. We revisit the question of MICI in the AIS using a more complex parameterization of cliff calving, which is based on the shear failure of an ice cliff and gives the cliff calving rate as an exponential function of ice thickness and water depth (**?**). A recent, more detailed modeling study of ice cliff failure, incorporating different structural failure modes as well as surface lowering due to viscous deformation, supports the findings that calving rates increase exponentially with ice thickness (**?**). In our model, we further assume that calved icebergs form an ice mélange that buttresses the ice cliffs, providing an upper bound on calving rates (**?**).

We consider the Amundsen region of the West Antarctic Ice Sheet (WAIS) as the likely initiator of MICI. Iceberg plow marks on the seafloor indicate that large full thickness icebergs calved from Pine Island Glacier and that MICI was active in this area during the last deglaciation (**?**). Additionally, the WAIS is grounded largely on bedrock below sea level and is therefore vulnerable to both the Marine Ice Sheet Instability (MISI) and MICI. MISI is caused by grounding line retreat on a retrograde bed: Retreat into deeper bed regions increases the flux across the grounding line and therefore accelerates grounding line retreat, resulting in self-reinforcing ice loss (**???**). Observations show that MISI is possibly already underway in the Amundsen region (**???**). Once MISI is initiated, the entire WAIS could collapse on a millennial time scale, resulting in sea level rise of 3 m (**?**). With the addition of cliff calving (MICI), the WAIS collapse would occur much more rapidly.

The breakup of ice shelves is a necessary precondition for the calving of exposed ice cliffs and thus for the onset of MICI. Hydrofracturing, in which the deepening of ice crevasses due to extensive surface meltwater leads to the catastrophic failure of an entire ice shelf, has been proposed by **?** as the main mechanism for ice shelf breakup and the consequent exposure of ice cliffs.
In 2002, the Larsen B ice shelf on the Antarctic Peninsula collapsed within a week after having thinned in previous years due to high summer melt rates (**??**). As a result of the ice shelf collapse, glaciers flowing into the shelf have permanently accelerated (**??**). These are small glaciers with little impact on the overall Antarctic mass balance. Based on the observation of numerous

surface meltwater ponds prior to ice shelf collapse, it has been suggested that hydrofracturing due to intense surface melting was the primary cause of this sudden collapse (**?**). However, anomalously large surface melt rates are required for an ice shelf to break up as rapidly as the Larsen B ice shelf did (**?**). Thus, hydrofracturing would probably not be the main mechanism leading to ice shelf failure in the Amundsen region: Even under the RCP 8.5 scenario, surface meltwater production on the Pine Island ice shelf is projected to remain far below a threshold of 300 mm/a at the end of the century (**?**). This threshold is equivalent to current surface meltwater production on the remaining Larsen C ice shelf and less than half of the pre-collapse surface meltwater production on the Larsen B ice shelf (**?**). Therefore, it is unlikely that the ice shelves in the Amundsen region will fail due to hydrofracturing.

Nevertheless, it is likely that the ice shelves in the Amundsen region will break apart under persisting global warming conditions. The Amundsen Sea is warming (**??**), leading to increased basal melting of ice shelves. This is already causing thinning and grounding line retreat in all the glaciers in the Amundsen region (**???**).
The destabilizing effect of basal melt on ice shelves can be further amplified by basal and surface crevasses: Satellite observations show a trend of widespread surface rifting at the shear margins of all glaciers in the Amundsen region (**?**) as well as an increase in rifts originating from basal crevasses in the center of the Pine Island ice shelf (**?**). Ocean warming may be the cause of the observed expansion of basal crevasses (**?**). Rifting and crevassing accelerates grounding line retreat: Damage feedback modeling showed that a basal melt rate of 20 m/a combined with a 20 m deep surface crevasse in the shear zone at the grounding line causes a faster grounding line retreat than a basal melt rate of 100 m/a on an undamaged shelf (**?**).
In addition, calving front retreat of small ice shelves may be self-reinforcing: a linear elastic fracture mechanics model of calving at Thwaites Glacier showed a positive feedback, i.e., if calving results in a shorter ice shelf, this shorter ice shelf is more likely to calve (**?**). It is also possible that weakened buttressing due to ice shelf thinning at Pine Island and Thwaites glaciers could amplify the development of damage in their shear zones. **?** suggest that this damage feedback may predispose the ice shelves at Pine Island and Thwaites glaciers for disintegration. This would remove buttressing from glaciers terminating in the Amundsen Sea and expose large ice cliffs, triggering MISI and MICI.

We perform a series of simulations using the Parallel Ice Sheet Model (PISM) in a regional setup of the WAIS, where we initiate MISI and MICI by removing the ice shelves in the Amundsen region. The ice sheet model and calving parameterizations are described in more detail in ~~see~~Sec. **??**. We present the resulting sea level contributions in ~~see~~Sec. **??**. In ~~see~~Sec. **??**, we discuss how the strength of mélange buttressing changes with grounding line retreat and show that as a result MICI slows down as it progresses.

2 Methods

2.1 Mélange-buttressed cliff calving

2.1.1 Model description

The model for mélange-buttressed cliff calving consists of two parts: a cliff calving parametrisation (**?**) and a mélange buttressing parametrisation (**?**).

For the ice cliffs, i.e. grounded ice sheet at the coast, we use a cliff-calving relation based on shear failure of an ice cliff (**?**). If the difference between ice thickness and water depths lies below a water depth dependent threshold ($\approx 100\,$m), the cliff is assumed to be stable. For larger ice cliffs, the calving rate grows exponentially with ice thickness and water depth. This assumed exponential relation and the fact that in many regions in West Antarctica the bed topography is down-sloping inland, can lead to very large calving rates ($> 30\,$km/a, see fig. **??**a).

In addition to the recently discussed stabilizing effect of dynamic thinning (**??**), a mélange of icebergs and sea ice, may have a stabilizing effect on MICI. Here we apply a very simple mélange-buttressing parameterization (**?**): Larger calving rates lead to the production of more icebergs, which together with sea ice form a stiff ice mélange. This mélange buttresses the ice cliff, thereby stabilizing it. As a result of this negative feedback between calving rate and mélange buttressing, there is an upper limit to the calving rate, C_{max} (see fig. **??**b). This threshold, derived in **?**, is a function of embayment geometry and mélange properties,

$$C_{max} = \frac{W_{ex}}{W_{cf}} \left(b_0 + b_1 \mu_0 \frac{L_{em}}{W_{em}} \right)^{-1} \gamma\, u_{ex}\,., \tag{1}$$

where the mélange length is denoted by L_{em}, the mélange width at the calving front by W_{cf}, the mélange exit width by W_{ex} and the average mélange width by W_{em} (see fig. **??**). γ is the fraction of the ice thickness H beyond which calving is completely suppressed, and u_{ex} is the exit velocity, with which mélange drifts out of the embayment. Finally, the internal friction of the mélange, μ_0, has values between 0.1 and 1 (**?**), and the linearization parameters are given by $b_0 = 1.17$ and $b_1 = 1.11$.

2.1.2 Uncertaineties in the model parameters

The scaling parameter in the cliff calving parameterization, C_0, is poorly constrained because it depends on the time scale of shear failure and there are no experimental or observational studies on this for ice (**?**). However, in the melange-buttressed case, C_{max} plays a much larger role in determining the overall calving rate, so the uncertainty of C_0 is not a major concern (**?**).

In the melange buttressing parametrisation, we chose $\mu_0 = 0.3$ and $\gamma = 0.2$ as in **?**. C_{max} depends linearly on the embayment exit velocity u_{ex} (see ~~eq~~Eq. **??**). Therefore, constraining its range is important for estimating C_{max}: Maximum mélange flow speeds observed in front of Greenland glaciers are $30 - 50\,\text{m/d} \approx 10 - 18\,\text{km/a}$ (**?**). The velocities of icebergs drifting in the Weddel Sea in Antarctica range from $9 - 15\,\text{km/d} \approx 3000 - 5500\,\text{km/a}$ (**?**). We assume that the mélange exit velocity lies within the range covered by these observations.

The value of C_{max} then depends solely on the embayment geometry (fig. **??**).

2.1.3 Mélange buttressing depends on embayment geometry

In order to estimate C_{max} for a given grounding line configuration, we assume that the entire embayment is filled with mélange. Note that the calving rate would be larger if the embayment ~~was~~ were initially free of mélange. However, since the mélange parameterization cannot evolve the mélange margin, we must assume its position. The evolution of the melange thickness can be modeled, though: When the entire embayment is filled with a very thin, spread-out mélange, the calving rate is high and many icebergs are produced. As a result, the melange thickness grows rapidly and reaches its equilibrium thickness within a few years (**?**). Therefore, it can be assumed that within a few years after the onset of calving, the entire embayment is filled with melange.

We estimate the width of the mélange exit, W_{ex}, and the length of the calving front, W_{cf}, by measuring the embayment manually. The average mélange width, W_{em}, is calculated as the average of W_{ex} and W_{cf}. The mélange length, L_{em}, is calculated as the average distance between the embayment exit and the calving front (the resulting trapezoids are shown in fig. **??**b). Tab. **??** shows estimates of C_{max} for Thwaites and Pine Island glaciers as well as for two extreme cases of mélange geometry: a narrow and long mélange strongly buttresses the calving front, resulting in a small C_{max}, while a wide and short mélange provides little buttressing at the calving front, resulting in a large C_{max}.

2.2 PISM

2.2.1 Model description

We carry out regional simulations of the WAIS with PISM (**??**) at a horizontal resolution of $4\,\text{km}$ and a minimum vertical resolution of $7\,\text{m}$. At this resolution, the reversibility of the grounding line is similar to that of higher-order models (**?**). The model setup is similar to the one used and described in **?**.

PISM is a thermomechanically coupled model based on the Glen–Paterson–Budd–Lliboutry–Duval flow law (**?**). It uses a superposition of the shallow ice approximation (**?**) and the shallow shelf approximation (**??**), allowing for a smooth transition between different ice sheet flow regimes. Basal friction is calculated using a nonlinear Weertman-type sliding law with a sliding exponent of 3/4 combined with a Mohr-Coulomb model for plastic till (**?**) that accounts for the effect of evolving ice thickness and the associated change in overburden pressure on the basal till. The till friction angle is parametrized with bed elevation (see **?**, eqs. 8-12). This friction scheme ensures a continuous transition from quasi–nonslip regimes in elevated regions to the marine areas where basal resistance is low. The grounding line position is free to evolve using hydrostatic equilibrium. Grounding line

Table 1. Upper bounds on calving rates given by ~~eq~~Eq. **??** with $\mu_0 = 0.3$, $\gamma = 0.2$ and $u_{ex} = 100\,$km/a. We first consider two extremes of a narrow and long as well as a wide and short buttressing mélange, while assuming a rectangular mélange geometry with constant mélange width, $W_{ex} = W_{cf} = W_{em}$. For Thwaites and Pine Island glacier, we assume mélange geometry similar to the current ice shelf. The smaller the upper bound C_{max}, the stronger the buttressing effect caused by the ice mélange.

	W_{em} [km]	L_{em} [km]	W_{ex}/W_{cf}	C_{max} [km/a]
narrow and long	5	100	1	2.6
wide and short	200	5	1	17.0
Thwaites Glacier	93	14	1.19	19.6
Pine Island Glacier	48	58	1.14	15.5

movement has been evaluated in the model intercomparison projects MISMIP3d (**??**) and MISMIP+ (**?**). Basal friction at the grounding line is interpolated according to a sub-grid, linear interpolation of the grounding line position (**?**).

2.2.2 Breakup of ice shelves

In our simulations, we assume that in the near future the ice shelves in the Amundsen region will break apart and will not be able to regenerate. This is a very strong assumption and is implemented in PISM with a so-called ’floatkill’ mechanism, which removes all floating ice in the Amundsen region at each time step. The ice front, which is now identical to the grounding line, is free to evolve. For the remaining ice shelves, mainly the Ross and Ronne-Filchner ice shelves, but also small ice shelves along the Antarctic Peninsula, the so-called eigencalving parameterization is applied (**?**).

2.2.3 Mélange-buttressed cliff calving

Mélange-buttressed cliff calving is applied to ice cliffs, i.e. grounded ice sheet at the coast. Similar to the ’floatkill’ parameterization, it is not applied to the entire model domain, but only to the coast of the Amundsen region and the interior of the WAIS. The shaded region in fig. **??** shows the region where the ’floatkill’ parameterization and mélange-buttressed cliff calving are not applied. This implementation prevents MISI and MICI from starting in other regions of the AIS, such as the Antarctic Peninsula.

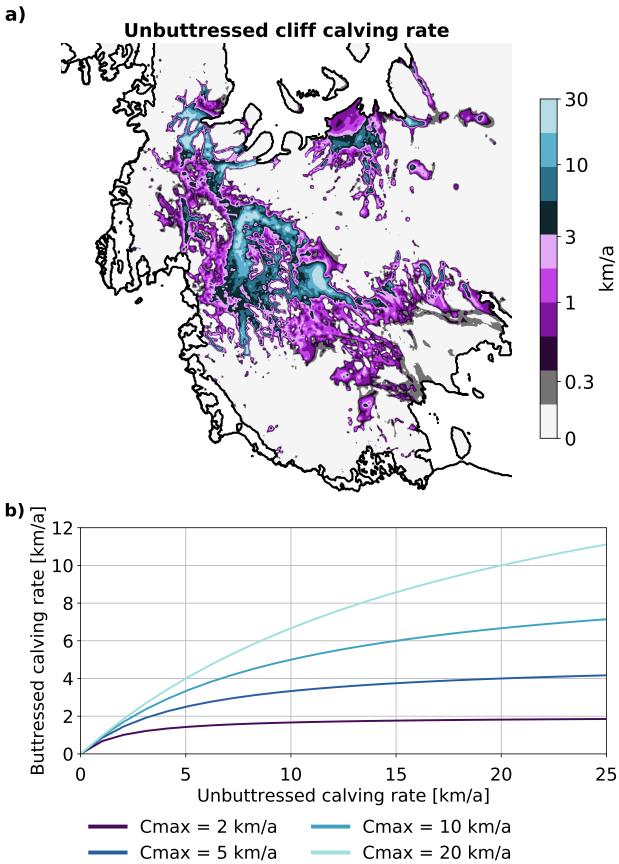

Figure 1. a) Potential unbuttressed cliff calving rates in the WAIS. For this estimate we assume the ice cliff to be at floatation thickness, making the calving rate a function of bed topography. In the case of very fast grounding line retreat, the ice cliff may not have thinned to floatation and calving rates may be larger. b) The mélange-buttressed calving rates as a function of the unbuttressed calving rates for the values of C_{max} considered in this study.

2.3 MISI and MICI in the WAIS with PISM

2.3.1 Boundary conditions

Basal melt rates under ice shelves are calculated using the Potsdam Ice-shelf Cavity mOdel (PICO) (**?**), where ocean conditions are determined by mean values over the observational period 1975-2012 (**?**). The surface mass balance and ice surface temperature are averaged from RACMO2.3p2 1986-2005 (**?**). The model domain includes the West Antarctic Ice Sheet, the Antarctic Peninsula and parts of the East Antarctic Ice Sheet, in particular the drainage basins towards Ross and Ronne-Filchner ice shelves (**?**). The bed topography and initial ice configuration were taken from Bedmap2 (**?**). For more details see **?**, where the same setup was used.

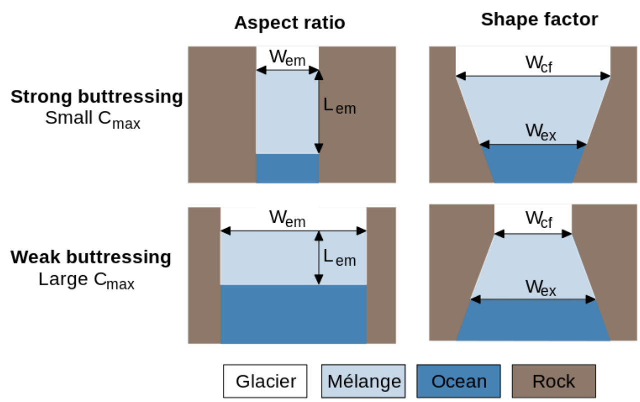

Figure 2. Illustration of how embayment geometry determines buttressing strength in ~~eq~~Eq. **??**: Aspect ratio L_{em}/W_{em} and shape factor W_{ex}/W_{cf} determine the strength of mélange buttressing.

2.3.2 Initialisation and experiments

The ice sheet was spun up into thermal equilibrium with fixed bed and ice geometry for 100,000 model years (**?**). A further 10-year run with evolving ice geometry was performed to remove short-lived floating regions in the WAIS (such as in the middle of Smith glacier, west of Thwaites glacier). Five types of experiments were carried out:

REF: a reference simulation with current day atmosphere and ocean conditions held constant (see ~~see~~Sec. **??**)

BMT: the 'basal melt experiment' is a melt experiment with current day atmospheric conditions and the melt rate in the Amundsen basin set to 200 m/a. This assumed basal melt rate is higher than the current and projected average melt rates of the Amundsen region ice shelves (**?**). However, close to the grounding line of Thwaites glacier, basal melt rates of up to 200 m/a were found (**?**). In the melt experiment, this rate was applied to the whole of the ice shelves in the Amundsen region. The ice front is free to evolve.

FLK: the 'floatkill'-parameterization experiment with current day atmospheric and ocean conditions, in which all floating ice in the Amundsen basin and the interior of the WAIS was removed. The grounding line is now the ice front and is free to evolve.

CC#: four cliff calving experiments, which were performed in the same way as the the 'floatkill'-parameterization experiment, with the addition of exposing grounded glacier margins to cliff calving with different upper limits. The upper bound range is $C_{max} = [2, 5, 10, 20]$ km/a (CC2, CC5, CC10, CC20).

CCA#: five adaptive cliff calving experiments, where the upper bound C_{max} was updated every 5 model years for the new embayment geometry. The mélange exit velocity range is $u_ex = [10, 50, 100, 200, 1000]$ km/a (CCA10, CCA50, CCA100, CCA200, CCA1000).

Each experiment was run for $100\,\mathrm{a}$. Some experiments (FLK, CC2, CC5, CC10, CCA10, CCA50, CCA100, CCA200) were extended until they reached a retreat comparable to the fastest cliff calving experiment (CC20).

2.4 Seasonal mélange freezing with the stand-alone mélange model

Finally, we investigated whether mélange freezing can stop MICI after its onset. Mélange freezing and thereby stopping calving has been observed in Greenland glaciers in the winter season (**?**). In the summer season, the sea ice in the mélange breaks up, the mélange becomes mobile and calving sets in again.

The mélange buttressing parametrisation can model melting of mélange as a loss of mélange volume and therefore mélange buttressing strength. However it cannot explicitly model mélange freezing. We used the exit velocity as a tool to simulate melange freezing: In the steady state model of mélange buttressing (see ~~see~~Sec. **??**), calving is completely suppressed if no mélange leaves the embayment exit ($u_{ex} = 0 \Rightarrow C_{max} = 0$, according to ~~eq~~Eq. **??**). However, starting with a very thin mélange and solving the non-state equations of the mélange-buttressing model as described in **?**, calving is allowed until the mélange thickness has reached its steady-state value.

We started from a very thin mélange ($10\,\mathrm{m}$) and modelled seasonality with a time-dependent mélange exit velocity of the form

$$u_{ex}(t) = u_0 \cdot \Big(1 + \arctan\left(k \cdot \sin(t \cdot 2\pi)\right)\Big) / \arctan(k) \quad \text{with } k = 20\,, \tag{2}$$

with a winter minimum of $u_{winter} = 0$, a summer maximum of $u_{summer} = 2u_0$ and an average of u_0.

The mélange geometry was assumed to be rectangular with $W = 30$km, $L = 60$km, the initial mélange thickness at the calving front was $d_0 = 10$m and the unbuttressed calving rate was $C_0 = 5$km/a.

3 Results

3.1 MISI discharge caused by ’floatkill’ is similar to that caused by basal melt

In our setup, the two MISI experiments (FLK and BMT) contribute about $0.6\,\mathrm{m}$ of sea level rise within $100\,\mathrm{a}$ (see ~~fig~~Fig. **??** and tab. **??**). This corresponds to the upper limit of the sea level contribution from the Amundsen sector found in LARMIP-2 (**?**), where a basal melt anomaly of up to $16\,\mathrm{m/a}$ was applied to currently observed melt rates. It is at the upper end of the 16 models that participated in LARMIP-2, but is not the highest.

The sea level contributions resulting from the FLK and BMT experiments are very similar. This agrees with results from the ABUMIP intercomparison study (**?**), which showed that Antarctic-wide ice loss due to large basal melt rates is comparable with ice loss due to the ’floatkill’ parameterization.

3.2 MICI discharge is controlled by upper bound on calving rates

When comparing the speed of the instabilities, we use two measures: the sea level contribution and the calving discharge. In the experiments with cliff calving (CC# and CCA#), MISI and MICI occur simultaneously. Therefore, the sea level contribution

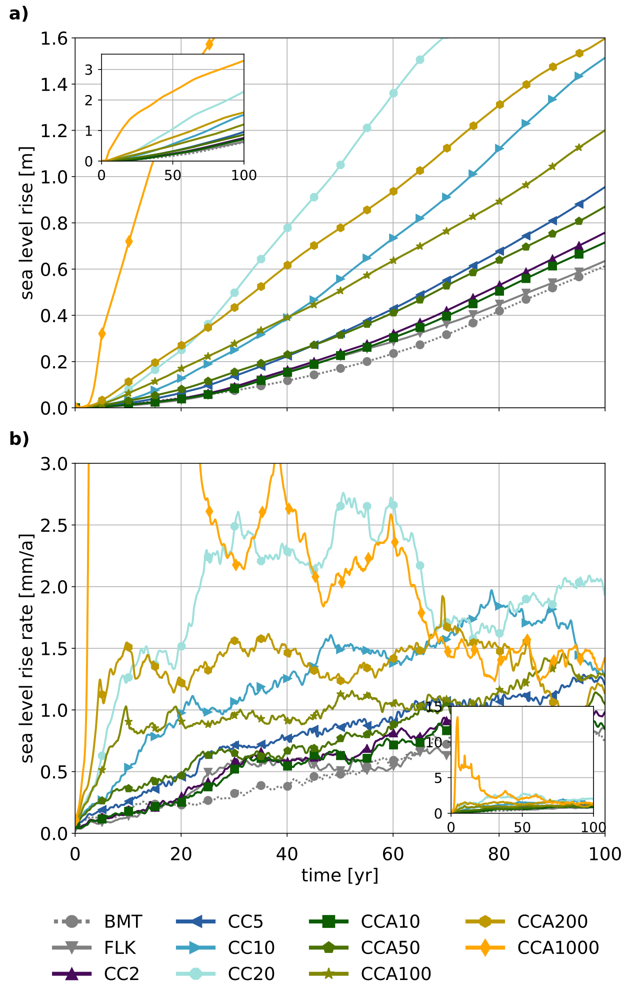

Figure 3. Cumulative sea level contribution (a) and rate of sea level rise (b) relative to the reference run for all experiments carried out. The insets shows the same plot but with a larger range so that the curve of the CCA1000 experiment is shown completely.

in these experiments is caused by both instabilities. Calving discharge is a better parameter to compare the contribution of MISI and MICI in each experiment because the discharge caused by the floatkill mechanism and the discharge caused by cliff calving are reported separately.

For the two lowest upper bounds on cliff calving (CC2 and CC5), MICI contributes a factor of up to 1.5 additionally to sea level rise from the MISI experiments. For larger upper bounds, MICI can more than double (CC10) or even triple (CC20) the sea level contribution compared to the MISI experiments (FLK, BMT). The sea level contributions of the first four adaptive experiments (CCA10, CCA50, CCA100, CCA200) are similar to those of the first three cliff calving experiments (CC2, CC5, CC10). The adaptive exeriment with the largest exit velocity (CCA1000) has more than five times the sea level contribution of

Table 2. Sea level contribution after 50 a and 100 a is comupted as the difference to the REF simulation. Cumulative calving discharge from the Amundsen region is given after 100 a. Average calving amplification is calculated as fraction between overall calving discharge (including cliff calving) and calving discharge only due to the 'floatkill' parameterization.

		sea level contribution [m] 50 a	sea level contribution [m] 100 a	cumulative discharge [10^6 Gt]	average calving amplification
MISI	BMT	0.17	0.61	-	-
	FLK	0.22	0.64	4.00	1
MISI + MICI	CC2	0.24	0.76	4.72	1.34
	CC5	0.32	0.95	6.00	1.86
	CC10	0.56	1.51	9.68	2.39
	CC20	1.05	2.28	14.53	3.15
	CCA10	0.23	0.72	4.34	1.22
	CCA50	0.31	0.87	5.43	1.63
	CCA100	0.51	1.20	7.64	2.02
	CCA200	0.78	1.60	10.14	2.38
	CCA1000	2.27	3.27	21.53	7.90

the MISI experiments (FLK and BMT) (see ~~fig~~Fig. **??** and tab. **??**).
Ice retreat rates increase with time, with sea level rates for the FLK and CC2 experiments reaching about 1 mm/a after 100 a, while the CC20 experiment reaches its maximum sea level rate of 2.5 mm/a already after 50 a. The sea level rate of the CC20 experiment decreases after 60 a of runtime because the grounding line retreat along the Pine Island Glacier towards the Ronne Ice Shelf has reached the boundary of the inner WAIS region, beyond which cliff calving and the 'floatkill' parameterization are not applied (see ~~fig~~Fig. **??**). In the adaptive experiments (CCA10, CCA50, CCA100, CCA200), the sea level rise rate increases initially and then levels off. This corresponds to the reduction of the adaptive upper bound on calving rates (see table **??** and ~~fig~~Fig. **??**). In the CCA1000 experiment, the sea level rise rate initially goes up to 13 mm/a and decreases sharply after 20 a when the retreat along the Pine Island Glacier reaches the boundary of the inner WAIS region where cliff calving and the 'floatkill' parameterization are applied. The sea level rate decreases again after 45 a when the retreat reaches bedrock above sea level and after 65 a when it reaches the boundary of the inner WAIS region close to the Siple coast (see ~~fig~~Fig. **??**).

Calving is the main cause of sea level rise: for experiments CC2, CC5, CCA10 and CCA50 the cumulative calving discharge is only slightly larger than for the FLK experiments; for experiments CC10 and CCA100 as well as CC20 and CCA200 the calving discharge doubles and triples, respectively. The slowdown of the CC20 experiment after 60 a is also visible in the reduced calving discharge. Similar to the sea level rise rate, the calving discharge of the adaptive experiments (CCA10, CCA50, CCA100, CCA200) increases intially and then levels off (see ~~fig~~Fig. **??** and tab. **??**).

For each cliff calving experiment (CC# and CCA#), PISM reports ice discharge due to the 'floatkill' mechanism and due to cliff calving separately. We use this to calculate the calving amplification as the ratio between the total calving discharge and the discharge only due to floatkill (tab. **??**). It reveals a doubling/tripling in the calving discharge for the highest values of C_{max}, similar to the increase in the sea level contributions mentioned above.

The cliff calving experiments with a small upper bound (CC2, CCA10) show only a modestly faster ice retreat compared to the 'floatkill' experiment. This is because PISM uses a subgrid scheme for the ice margin, involving partially filled cells that are not affected by either the ice dynamics or the 'floatkill' mechanism (**?**). Cliff calving with a small value of C_{max} can prevent partially filled cells from filling up and thus reduce the ice loss due to the 'floatkill' parameterization. This may result in a slightly lower overall calving discharge compared to 'floatkill' with no cliff calving. Cliff calving with a large value of C_{max} is much more likely to completely remove partially filled cells, so the 'floatkill' parameterization mechanism is not hindered in this case. This issue depends on the resolution of the domain: Previous unpublished sensitivity tests in a channel setup showed that for a resolution of x km, this problem occurs for calving rates smaller than x km/a.

3.3 Mélange buttressing increases as MICI progresses, slowing MICI speed

In the adaptive cliff calving experiments (CCA#), mélange buttressing strength depends on the embayment geometry (see ~~eq~~Eq. **??** and ~~fig~~Fig. **??**). Because the calving front becomes longer and its distance to the embayment exit increases, the upper bound on calving rate decreases with grounding line retreat into the Amundsen basin. The development of the upper bound with simulation time is given in table **??**. In fig **??**, the upper bound is shown as a function of the sea level contribution of the corresponding embayment geometry. Initially, Thwaites and Pine Island glacier have separate embayments with different values for C_{max}. After some time depending on the mélange exit velocity, the embayments merge, leading to one value of C_{max} for the whole Amundsen basin. As the grounding line retreats deeper into the Amundsen basin, C_{max} decreases to about one third of its initial value. The relation between calving rate and sea level contribution can be fitted with:

$$\frac{C_{max}}{C^0_{max}} \approx 0.19 \cdot \exp\left(\frac{0.17\,\mathrm{m}}{\mathrm{SLR} + 0.11\,\mathrm{m}}\right). \tag{3}$$

with C^0_{max} the average of the initial upper bounds for Thwaites and Pine Island glacier.
As MICI progresses and the grounding line retreats, the area covered by ice mélange grows, which increases the strength of mélange buttressing. This in turn lowers the upper limit on calving rates and slows further progression of MICI. Thus, as a consequence of mélange buttressing, MICI cannot be arbitrarily fast and even decelerates as it progresses.

3.4 Bed topography controls rate of grounding line retreat

The grounding line retreat initially follows the main flow directions of Pine Island and Thwaites glaciers, but after some time (depending on C_{max}) it involves the entire interior of the WAIS (see ~~fig~~Fig. **??**). The retreat reaches the Ronne Basin earlier

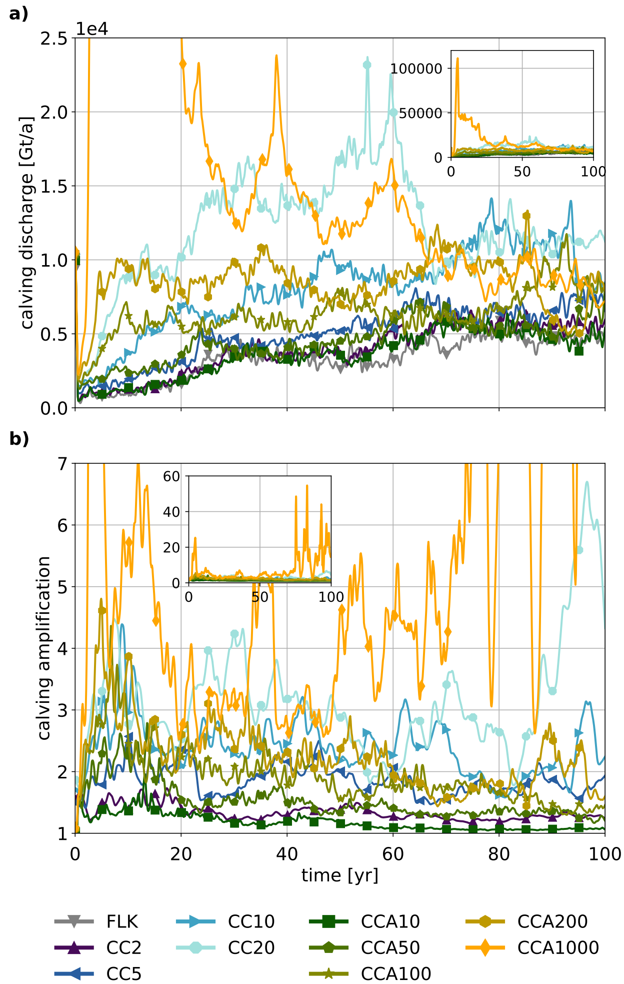

Figure 4. a) Overall calving discharge from the Amundsen region. PISM uses a subgrid scheme at the ice margin with partially filled cells (**?**). At each time step, calving removes some of the ice in such a cell, while floatkill removes whole cells if they float. This removed ice volume is summed up in the calving discharge variable. b) The calving amplification calculated as the fraction between overall calving discharge and calving discharge due to the 'floatkill' parameterization only. Note that no calving amplification has been calculated for the 'floatkill'-only experiment because no cliff calving takes place. The calving amplification of the CC20 and the CCA1000 experiments increases toward the end of the simulation time because parts of the grounding line have reached the margin of the inner WAIS region, beyond which cliff calving and the 'floatkill' mechanism are not applied.

than the Ross Basin. The CC20 experiment reaches the Ronne Ice Shelf after 70 a of runtime, where the retreat ends as no further the 'floatkill' parameterization and cliff calving is allowed there. The retreat towards the Ross Ice Shelf continues. The experiments with smaller C_{max} as well as the FLK experiment take longer to reach the Ronne Ice Shelf, with the FLK

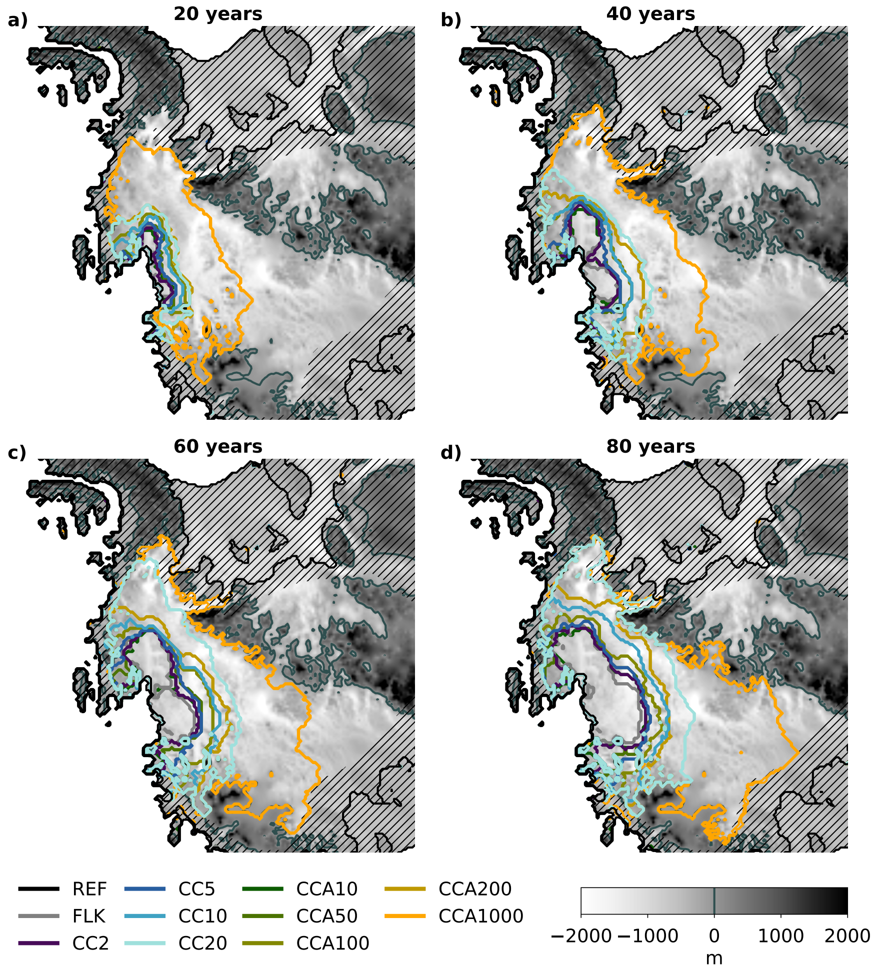

Figure 5. Maps of grounding line retreat in the WAIS, underlaid with the bed topography. In the shaded region, neither the 'floatkill' parameterization nor cliff calving is applied (see ~~see~~Sec. **??**). Grounding line retreat of CCA1000, the fastest experiment, halts when it reaches bed topography above sea level (in which case cliff calving is no longer applied) or the margin of the interior Amundsen region domain (beyond which neither floatkill nor cliff calving are applied).

experiment being the slowest, arriving there after 150 a.(not shown here).

We examine the retreat along two flowlines, leading from Thwaites glacier across to Ross ice shelf and from Pine Island glacier across to Ronne ice shelf, respectively (see ~~fig~~Fig. **??**). These are the same 2d-experiments discussed in the rest of the paper, except that they are analyzed along the trajectory of the flowlines. Since the ice divides are free to move, it may be that their lateral movement changes the actual flowline, i.e., the main direction of the ice flow. This has not been taken into account. Both glaciers have retrograde beds, with Thwaites glacier having a steeper slope than Pine Island glacier. After the flowlines

Table 3. Upper bound on calving rates for the adaptive cliff-calving experiments (CCA#) in km/a. Where two values are given, the first is for Thwaites glacier and the second for Pine Island glacier. Where only one value is given, both glaciers share one embayment.

	0 a	20 a	40 a	60 a	80 a	100 a
CCA10	1.96 / 1.55	1.51 / 1.85	1.48 / 1.26	0.60	0.54	0.50
CCA50	9.78 / 7.75	4.09	2.97	2.77	2.67	2.30
CCA100	19.6 / 15.5	7.72	5.90	5.32	4.98	4.57
CCA200	39.1 / 31.0	12.6	9.23	8.61	7.28	6.78
CCA1000	195 / 155	32.2	25.5	21.3	22.3	21.4

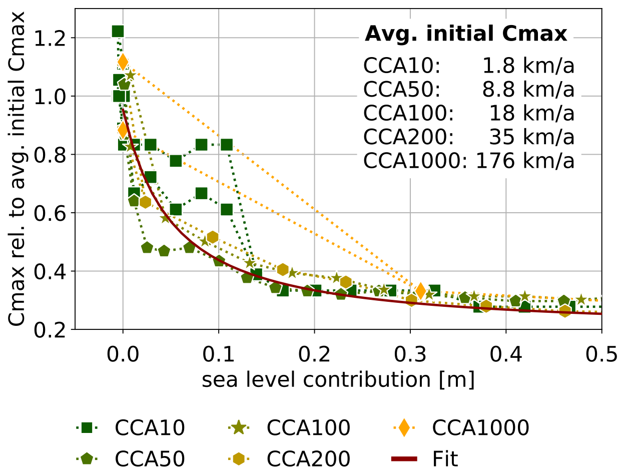

Figure 6. The upper bound on calving rates, C_{max} of the adaptive cliff calving experiments (CCA#) as a function of the sea level contribution of the corresponding embayment geometry. Initially, Thwaites and Pine Island glacier have separate embayments, which merge after several model years. The upper bound decreases with sea level contribution and with the corresponding simulation time (see table **??**).

cross the initial ice divide, the bed topography changes: The retreating grounding line of Thwaites Glacier meets the Bindschadler Ice Stream, which has a rather shallow and slightly prograde bed topography (in the direction of grounding line retreat). In contrast, the retreating grounding line of Pine Island glacier reaches the Evans Ice Stream, which has a deep bed depression. Fig. **??** shows the retreat of the grounding line and ice divide along these flowlines over time. For Thwaites glacier, all experiments show some inertia to the retreat initially, which is followed by rapid retreat along the first 150 km of the flowline. Retreat then levels off, with experiments with larger C_{max} showing faster retreat. Pine Island glacier shows steady initial retreat over the first 300 km, after which the retreat stalls for 25 a to 50 a, depending on the experiment. This is followed by a rapid retreat that is stopped only when the grounding line reaches the Ronne Ice Shelf, where no further retreat is possible. As

Table 4. Upper bound on calving rates for the adaptive cliff-calving experiments (CCA#) in km/a. Where two values are given, the first is for Thwaites glacier and the second for Pine Island glacier. Where only one value is given, both glaciers share one embayment.

	0 a	20 a	40 a	60 a	80 a	100 a
CCA10	1.96 / 1.55	1.51 / 1.85	1.48 / 1.26	0.60	0.54	0.50
CCA50	9.78 / 7.75	4.09	2.97	2.77	2.67	2.30
CCA100	19.6 / 15.5	7.72	5.90	5.32	4.98	4.57
CCA200	39.1 / 31.0	12.6	9.23	8.61	7.28	6.78
CCA1000	195 / 155	32.2	25.5	21.3	22.3	21.4

the grounding line retreats, so does the ice divide, but with a considerable delay.

An explanation for this retreat pattern can be found by a more detailed analysis that compares the grounding line retreat rates with the slope of the bed topography (see ~~fig~~Fig. **??**). Grounding line retreat along the Thwaites flow line is rapid at first, with retreat rates up to $18\,$km/a (depending on C_{max}) along a steep retrograde bed, and slows down once the grounding line reaches a more even bed topography segment beginning at $150\,$km. In this segment, retreat rates fluctuate below $10\,$km/a. Ridges in the bed topography at $220\,$km and $430\,$km cause stagnation of grounding line retreat on the upslope, followed by acceleration on the downslope. A steady retrograde slope between $500\,$km and $630\,$km causes grounding line retreat rates to increase up to $10\,$km/a. The steep prograde slope between $630\,$km and $700\,$km causes the retreat to slow down significantly.
The retreat along the Pine Island flow line has a steady rate between $5\,$km/a and $15\,$km/a for the first $300\,$km until the grounding line approaches a bathymetric ridge, where the retreat slows temporarily. A short $20\,$km long depression following this ridge causes an acceleration of up to $10\,$km/a, followed by a slowdown as the bed rises again. Grounding line retreat accelerates sharply up to values between $15\,$km/a and $33\,$km/a once it reaches a steep bed depression beneath Evans ice stream, which begins at $450\,$km.
The CCA1000 experiment has much larger calving rates than the other experiments (see table **??**) and therefore also much larger retreat rates. Its retreat depends more on the mélange buttressing than the bed topography.

We expect bed topography to control grounding line retreat for two reasons: analytical calculations in a depth-averaged flowline model show that the flux across the grounding line scales superlinearly with ice thickness (**?**). The cliff calving rate also scales superlinearly with ice thickness (**?**). Assuming that the glacier terminus is at floatation, this means that there should also be a relationship between the grounding line retreat rate and the bed depth.
However, a correlation analysis using the Spearman correlation coefficient of determination between grounding line retreat rate and bed topography shows only a minimal correlation for Pine Island Glacier and no correlation at all for Thwaites Glacier (see tab. **??**). There are two main reasons for this: First, we analyze flow along a 1d flowline embedded in a more complex 2d

Table 5. Spearman correlation coefficients of determination between bed depth and grounding line retreat rate.

		Thwaites Glacier	Pine Island Glacier
MISI	FLK	0.06	0.79
MISI + MICI	CC2	0.04	0.80
	CC5	0.07	0.76
	CC10	0.04	0.77
	CC20	0.01	0.64
	CCA10	0.08	0.73
	CCA50	0.07	0.52
	CCA100	0.01	0.62
	CCA200	0.13	0.50
	CCA1000	0.01	0.37

flow. The retreat of the grounding line in neighboring flowlines, where the bed topography can be different, may drag on the grounding line and either accelerate or decelerate it, in comparison to the result of the 1d analysis. In addition, the analyzed flowlines may not lie exactly along the flow direction, especially in the vicinity of bed topography disturbances that are only a few grid cells in size. Second, ice flow has inertia, which means that the grounding line takes some time to accelerate when it reaches a steep retrograde bed. Inertia can also drive it over bumps in the bed that would be expected to slow it down, especially in the case of large C_{max}.

In summary, we find no clear statistical correlation between the bed topography and the grounding line retreat rate. Nevertheless, we observe an acceleration of the grounding line when the bed is retrograde and a deceleration when it is prograde. In addition, bathymetric ridges temporarily halt grounding line retreat. So we can conclude that bed topography is a major control on the rate of grounding line retreat.

3.5 Winter freezing of mélange is not sufficient to stop MICI

Asuming that no mélange exits the embayment, mélange buildup can prevent calving almost completely within 10 a (see ~~fig~~Fig. **??**a, grey lines). Assuming a seasonal exit velocity leads to seasonal variations in the strength of mélange buttressing (see ~~fig~~Fig. **??**, orange and blue lines): After an initial equalibration period, mélange volume and backstress decrease in the summer and the calving rate increases, while in the winter mélange volume and backstress increase and the calving rate decreases. The minimum and maximum mélange properties fluctuate around the equilibrium value calculated by using the averaged exit velocity u_0. Contrary to observations, in this simplified mélange parameterization, winter freezing of mélange is not sufficient to

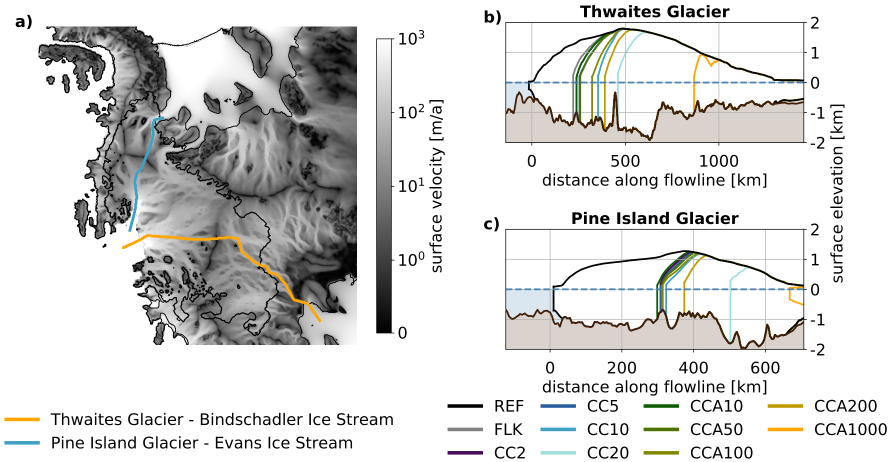

Figure 7. a) Map of flowlines from Pine Island glacier through Evans ice stream to Ronne ice shelf and from Thwaites glacier through Bindschadler ice stream to Ross ice shelf. b) and c) Bed topography and ice surface profiles after 60 a runtime for Thwaites glacier and Pine Island glacier, respectively. The distance along the flowline has its zero at the initial grounding line position. Note that for Pine Island glacier, the reference run also shows some grounding line retreat.

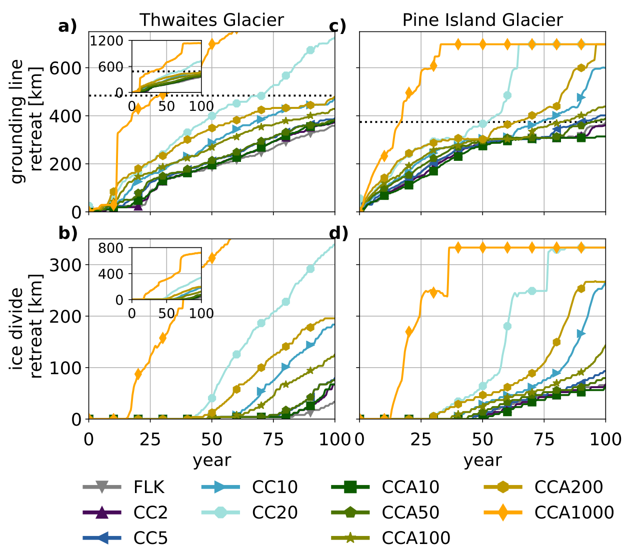

Figure 8. Grounding line retreat (a and c) and ice divide retreat (b and d) along the flowlines in Thwaites (a and b) and Pine Island glacier (c and d) as a function of simulated time. The dotted line shows the initial ice divide position.

stop calving. The reason is that the equilibration of the mélange is too slow and takes several years rather than months or weeks.

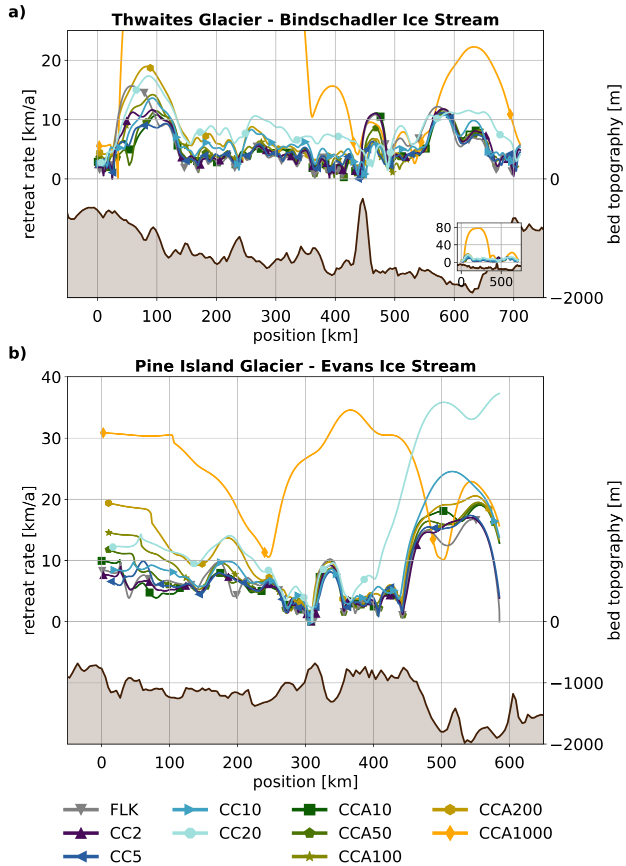

Figure 9. Grounding line retreat rates along the flowlines in Thwaites (a) and Pine Island glacier (b) as a function of grounding line position, together with bed topography. Markers are set every 10 a.

Studies explicitly analysing the influence of the mélange backpressure on the stress balance of the glacier terminus focus on the the force per unit width exerted by the mélange at the calving front (**???**). Therefore, the force per unit width was calculated as a diagnostic variable. A mélange backpressure of $6.66 \cdot 10^6$ N/m is sufficient to prevent cliff calving of an ice cliff with $H = 1000$ m (**?**). In our solution of the non-steady state equation, a similar force per unit width was found when calving is suppressed (see ~~fig~~Fig. **??**c, grey lines after > 5 a).

In conclusion, assuming that no mélange is lost by drifting off at the mélange exit, a very thick and strong mélange is built up within a period of several years, which completely prevents further calving and would thus stop the progression of MICI. However, this is only likely to happen in the winter season and would therefore halt MICI only temporarily.

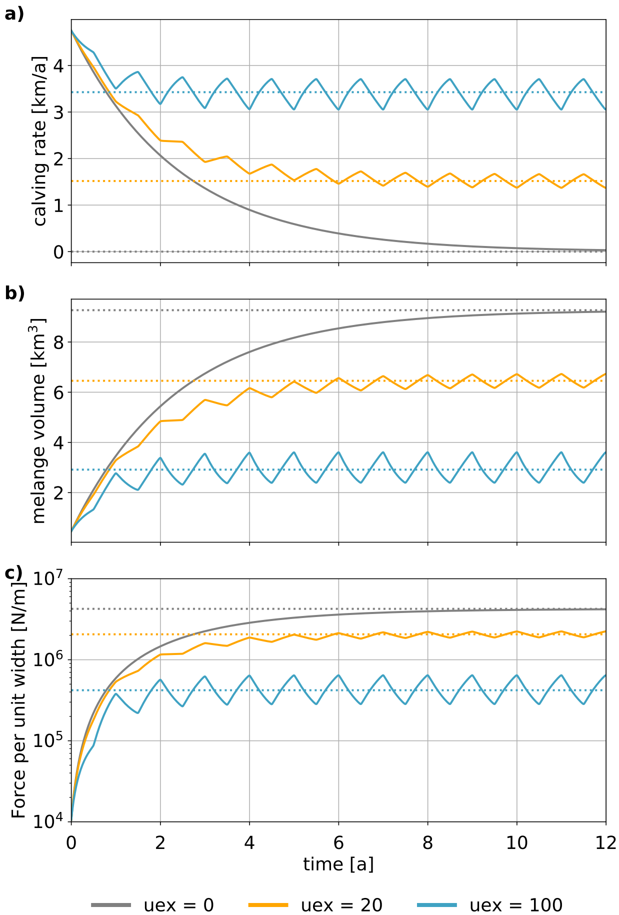

Figure 10. Evolution of the buttressed calving rate (a), the mélange volume (b) and the force per unit width at the calving front (c) in the case of no mélange exiting the embayment ($u_{ex} = 0$, grey lines) and for a seasonal variation in mélange exit velocity (orange and blue lines). The dotted lines show the corresponding equilibrium solution. For an equalibrated ice mélange, if no mélange exits the embayment ($u_{ex} = 0$), calving is completely suppressed ($C_{max} = 0$). However, in the time-dependent case and starting with a thin initial mélange, calving is possible for some years. Seasonal variations in the exit velocity lead to a seasonal variations of the mélange buttressing strength.

4 Discussion

In this section we discuss our results in the light of mechanisms and conditions that may be important in limiting the speed of MICI evolution, including the influence of melange properties, climatic variations, and the ice/bed geometry.

4.1 Limitations of the idealized mélange buttressing parametrization

Due to its reliance on an idealized geometry, the mélange parametrization has several limitations when applied to realistic embayment geometries (see figs. **??**a and b):

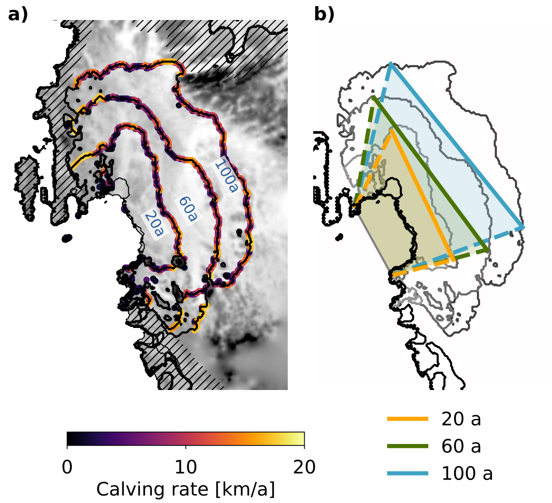

Figure 11. a) Different grounding line configurations of the adaptive cliff calving experiment CCA100 with unbuttressed calving rates. b) Idealized embayment geometry derived from the grounding lines.

- The conversion of the realistic geometry into the idealized geometry is not unique: It is difficult to specify exactly where each parameter of the idealized geometry should be measured.
- The mélange parameterization assumes a constant calving rate along the entire length of the calving front. This may be valid when considering a single glacier, but is no longer the case when several glaciers calve into the same embayment.
- On the west side of the Amundsen embayment, ice resting on bedrock above sea level forms pinning points that provide additional support to the ice mélange. This effect is neglected in the parameterization.
- The mélange margin cannot be inferred from the model and must therefore be provided as an external parameter.
- Mélange freezing cannot be modelled explicitly and has been modelled using the mélange exit velocity. This allows mélange buildup, but its effect takes too long to transmit to the calving front (several years).

To get a better understanding of how mélange buttressing impacts calving rates in a realistic setup, it would be beneficial to use a spatially resolved mélange model. It should be able to handle realistic embayment geometries including pinning points as well as spatially resolved calving rates and have a criterion for where mélange stops being mélange, which would enable it to model the mélange margin (see e.g. **?**). However, such a model introduces additional mélange parameters, which are difficult to constrain.

4.2 The role of ice shelves for MICI

Understanding the processes by which ice shelves fracture rapidly and disintegrate is still ongoing work (**???**) and difficult to be implemented in an ice sheet model.

One way to remove ice shelves is by highly elevated basal melting. In PISM, this approach leaves small ice shelf remnants that are only a few grid cells in size. The resulting buttressing loss induces MISI. However, since we assume that cliff calving only occurs at exposed, grounded ice cliffs, the ice shelf remnants prevent the onset of MICI. This is in contrast to the implementation in **?**: They assumed that a small ice shelf remnant with vanishing buttressing strength does not prevent cliff calving, basing their reasoning on the Schoof flux across the grounding line (**?**) and depth-averaged stresses in vicinity of the ice cliff (**?**). However, the Schoof flux may not be applicable beyond a flowline setup (**?**). Additionally, a small ice shelf may impact the stress balance at the ice cliff in a 3d-setup. Therefore, we assume that cliff calving only occurs at exposed grounded ice cliffs. In our model setup, we remove all floating ice in the Amundsen Basin and inner WAIS. This 'floatkill' parameterization mechanism eliminates all existing ice shelves at once in the first time step and prevents re-growth of ice shelves during the retreat. The removal of ice shelves initiates both MISI and MICI.

Two questions of vital importance for the onset and progress of MICI need further research:

1. Under which conditions do ice shelves collapse completely? Since ice shelf collapse is the prerequisite for the onset of MICI, the answer to this question determines when and if at all MICI will play a role for the future of the Antarctic ice sheet. There has been a lot of observational and theoretical work on hydrofracturing (**??**) as well as rifting and crevassing (**???**), but so far it is impossible to predict under which environmental and internal conditions a specific ice shelf will collapse.

2. Can ice shelves regrow after MICI has set in? If ice shelves can regrow after cliff calving has begun, this could stop MICI after its onset by buttressing the ice cliffs and preventing further cliff calving. However, if ice shelves cannot regrow, then MICI will continue mostly unhindered, because mélange buttressing can only slow the progress of MICI, but not stop it. Viscous deformation could prevent the formation of unstable ice cliffs (**??**) and allow ice shelves to regrow, whereas a mixed-mode behaviour of viscous deformation and fracture (**?**) would make ice shelf regrowth unlikely.

4.3 Influence of regional climatic conditions on the progress of MICI

So far there are few observations of cliff calving glaciers. The retreat of Sermeq Kujalleq, also known as Jakobshavn glacier **?**, in Greenland since 1998 (**?**) was regarded as an indication that Sermeq Kujalleq may be at the beginning of cliff calving regime (**???**). However, since 2016, Sermeq Kujalleq has re-advanced as a result of regional ocean cooling (**?**). The cooling of the Fjord water has led to a decrease in frontal melt (**?**) as well as increased mélange buttressing at the glacier terminus (**?**), thereby stopping its retreat. This suggests that changes in regional climatic conditions may slow or prevent grounding line retreat caused by cliff calving.

4.4 Slowdown of MICI at bathymetric ridges

During the last deglaciation, MICI was probably active for approximately $1000\,\mathrm{a}$ in the Amundsen region of the WAIS and then stopped, when the grounding line re-stabilized on a prominent bathymetric ridge (**?**). This is an indication that MICI can be stopped after its onset by features of the bed topography. However, our simulations show only temporary halts in grounding line retreat at bathymetric ridges in the interior of the WAIS (see ~~fig~~Fig. **??**).

5 Conclusions

We performed PISM simulations of the WAIS to investigate the potential speeds of the two marine instabilities, MISI and MICI. We choose the Amundsen region as the starting point of the instabilities because observations show that MISI is possibly already in progress there. Due to ocean warming and increased crevassing, glaciers in the Amundsen region may lose their ice shelves in the future, which would set MICI in motion. We applied a 'floatkill' parameterization to remove the ice shelves in the Amundsen region, a cliff-calving parameterization depending on ice thickness, and a mélange-buttressing parameterization which limits calving rates.

We found that MISI, whether forced by the 'floatkill' parameterization or by high subshelf melt rates, has the potential to contribute 0.6 m of sea level rise within 100 a. The sea level potential of MICI depends on the upper limit of calving: if the cliff calving rate is limited below 2 km/a or 5 km/a, MICI has a smaller contribution to sea level rise than MISI. If the upper limit is 10 km/a or 20 km/a, MICI doubles or even triples the sea level contribution of MISI.

We also showed that grounding line retreat is regulated by bed topography for both MISI and MICI. Although there is no clear statistical correlation between the retreat rate and the bed depth, we observe an accelerated retreat of the grounding line on retrograde beds and a slowdown on prograde beds.

Finally, we investigated how the upper limit for calving from mélange buttressing depends on the embayment geometry and the mélange exit velocity. Seasonal effects cause mélange build-up, which slows the progress of MICI temporarily under winter condition. We also showed that as MICI progresses and the grounding line retreats, the calving front becomes longer while the width of the embayment exit remains the same. This leads to an increase in mélange buttressing, a decrease in the upper bound on calving rates, and consequently a slowdown in the progress of MICI. It is unlikely that mélange alone can completely stop MICI, but it could provide enough buttressing to enable ice shelf regrowth, which would then stop further MICI progress.

Future research is needed to gain a better understanding of the conditions under which MICI kicks off and to further constrain its potential sea level contribution.

The applied mélange parameterization assumes an idealized geometry and is therefore of limited applicability when extended to realistic embayment geometries. A spatially resolved mélange model might be a better choice. However, such a model would require more parameters describing mélange properties, which are difficult to constrain.

Two important unresolved questions about ice shelf collapse are beyond the scope of this study: first, under which conditions do ice shelves collapse? This determines the onset of MICI and is therefore crucially important in constraining at what degree of warming MICI becomes a concern. Second, can ice shelves regrow after MICI has started? This seems to be the only way to stop MICI. These two important questions control if and when MICI sets in and if it can be not only slowed down, but stopped completely after its onset.

Code and data availability. The PISM code used for these simulations is available at https://doi.org/10.5281/zenodo.6325006. The model output data and python scripts for running the experiments and generating the figures shown in the paper are stored in a band archive at the Potsdam Institute for Climate Impact Research and indexed in a metadata archive; they are available upon request.

Author contributions. TS and AL designed the study with input from RW. JF created the regional setup of the WAIS and performed the spinup. TS performed the simulations, analyzed the model results, and wrote the manuscript. All authors commented on the manuscript.

Competing interests. We have no competing interests.

Acknowledgements. This paper is supported by European Union's Horizon 2020 research and innovation programme under grant agreement No 869304 (PROTECT). This paper is supported by European Union's Horizon 2020 research and innovation programme under grant agreement No 820575 (TiPACCs). JF and RW acknowledge support by the Deutsche Forschungsgemeinschaft (DFG) through grants WI4556/4-1 and WI4556/6-1. RW is grateful for support by European Union's Horizon 2020 research and innovation programme under grant agreements No 820575 (TiPACCs) and No 869304 (PROTECT), and by the PalMod project (FKZ: 01LP1925D), supported by the German Federal Ministry of Education and Research (BMBF) as a Research for Sustainability initiative (FONA).